

Electrochemical Micromachining

Rolf Schuster,^{1*} Viola Kirchner,¹ Philippe Allongue,²
Gerhard Ertl¹

The application of ultrashort voltage pulses between a tool electrode and a workpiece in an electrochemical environment allows the three-dimensional machining of conducting materials with submicrometer precision. The principle is based on the finite time constant for double-layer charging, which varies linearly with the local separation between the electrodes. During nanosecond pulses, the electrochemical reactions are confined to electrode regions in close proximity. This technique was used for local etching of copper and silicon as well as for local copper deposition.

The machining of materials on micrometer and submicrometer scales is considered to be a key future technology. Aside from the well-known lithographic processes used in the fabrication of electronic devices, micromachining technologies play an increasing role in the miniaturization of complete “machines” (1, 2) ranging from biological and medical applications (3, 4) to electro-mechanical sensors and actuators (5) to chemical microreactors (6, 7). Lithographic processes were successfully combined with electrochemical methods in the LIGA process (8), in which small mechanical parts are electrodeposited into a lithographically structured polymer mask [LIGA is the acronym for the German expressions for the three main process steps: lithography (LI), electroforming (G), and molding (A)]. Although lithographic methods allow the successful implementation of mostly two-dimensional (2D) structures down to the lower nanometer scale, the fabrication of structures with high aspect ratios or even 3D topography has hitherto been an only partly solved challenge: Ion beam milling or deposition has proven to be able to machine various materials down to the nanometer range but suffers from relatively slow speed because of the sequential processing. With 3D anisotropic etching of Si surfaces, the geometrical shape of the structures is determined by the crystal structure of the substrate. Extending laser ablation techniques or mechanical methods such as drilling or milling into the nanometer range is still on the edge of today’s technology (1).

Here we present a method by which electrochemical reactions on conducting materials can be localized with submicrometer precision. An appropriately shaped tool electrode is directly molded on the workpiece, either by local etching or

local electrodeposition of material. 3D control of the tool electrode position enables direct 3D micromachining with very sharp resolution. This is achieved by the application of ultrashort voltage pulses of only nanosecond duration. In this case, the time constant for charging the double layers (DLs) on the electrodes (that is, the product of electrolyte resistance and DL capacity) is small enough for significant charging only at electrode separations in the nano- to micrometer range. Because the rates of electrochemical reactions are exponentially dependent on the potential drop in the DL, the reactions are strongly confined to these polarized electrode regions in very close proximity. This method contrasts with conventional electroforming methods, in which the application of DC voltage causes uniform DL charging and the reaction rate is mainly defined by the current density in the electrolyte, thus enabling only limited spatial resolution of about 0.1 mm. Our approach also differs from recent methods combining scanning probe techniques and electrochemical methods for surface structuring (9). In those methods, the spatial resolution stems from limited diffusion of the electrolyte ions (10–15), mechanical modifications by the electrochemically modified tip apex (16), or geometrical confinement of the electrolyte volume (17, 18).

The concept of our method can be illustrated by a simplified equivalent circuit of two electrodes immersed in electrolyte (Fig. 1A). On both electrodes, the electrochemical DL constitutes a capacity, which is charged upon application of a voltage step between the electrodes. The charging current has to flow through the electrolyte, whose resistance is proportional to the length of the current path; that is, the distance between the electrodes. This leads to locally varying time constants $\tau = RC = \rho dc_{DL}$ for the charging of the DL, depending on the (local) separation d between the electrodes, the specific electrolyte resistivity ρ , and the specific DL capacity c_{DL} . Upon application of a voltage pulse, the electrodes will only be significantly

charged where the local τ does not substantially exceed the pulse duration. Hence, with short enough pulses, the polarization of the DL will reach appreciable values only near the very tip of the tool electrode, where both electrodes are in close proximity and the electrolyte resistance (R) along the current path is low (R_{close}). In contrast, the regions further out (R_{wide}) become only weakly polarized. Therefore, the electrochemical processes, whose rate is exponentially dependent on the potential drop in the DL, will be sharply confined to electrode regions in close proximity to the tool. With typical values of $\rho = 30 \text{ ohm} \cdot \text{cm}$ (0.1 M HClO_4) and $c_{DL} \approx 10 \text{ } \mu\text{F}/\text{cm}^2$ for metal electrodes (19, 20) and pulse durations of $T = 30 \text{ ns}$, this maximum distance d , where significant charging of the DL is achieved, calculates to $d \approx 1 \text{ } \mu\text{m}$. Pulses of 30 ns duration should therefore achieve a machining resolution of about 1 μm .

Experimental verification of this concept was achieved when a Cu substrate was immersed in an electrochemical cell mounted on a piezo-driven x - y - z stage (Fig. 1B). For monitoring the absolute position of the workpiece with respect to the tool electrode, the piezo stage was equipped with strain gauges. The tool was a cylindrical Pt wire (10 μm or 50 μm in diameter), whose front face was flattened by mechanical pol-

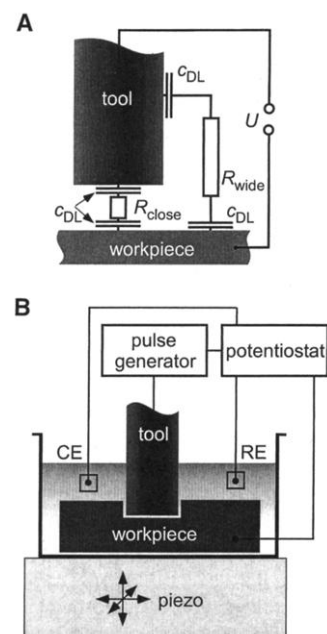


Fig. 1. (A) Scheme of an electrochemical cell. Upon application of a voltage pulse, the DL capacity c_{DL} is charged via the electrolyte resistance. Because the electrolyte resistance along the current path depends on the electrode separation (R_{close} and R_{wide}), the time constants for charging the DL become spatially varying. (B) Experimental setup for electrochemical micromachining with ultrashort voltage pulses.

¹Fritz-Haber-Institut der Max-Planck-Gesellschaft, Faradayweg 4-6, D-14195 Berlin, Germany. ²Physique des Liquides et Electrochimie, CNRS UPR 15, 4 Place Jussieu, F-75005 Paris, France.

*To whom correspondence should be addressed. E-mail: schuster@fhi-berlin.mpg.de

ishing after the wire was embedded in redissolvable resin. Both electrode potentials were controlled with a low-frequency bipotentiostat (time constant ≈ 1 ms) versus a pseudo reference electrode (RE) made of a Pt wire. The electrolyte was an aqueous mixture of HClO_4 and CuSO_4 . The sample potential was kept at the well-defined equilibrium potential of $\text{Cu}|\text{Cu}^{2+}$. This ensured that the workpiece corroded only negligibly during the experiment. The average potential of the tool electrode was adjusted to 200 mV versus $\text{Cu}|\text{Cu}^{2+}$. For local etching, a sequence of 50-ns, -1.6 -V pulses with a pulse-to-pause ratio of 1/10 was applied to the tool electrode. The bipotentiostat was unaffected by the short pulses and therefore only controlled the average workpiece and tool potentials. Furthermore, during the short pulse, the charging current flowed essentially between tool and workpiece because of the very small distance between tool and workpiece (micrometers) compared with the large distance between the counter electrode and the tool or workpiece (millimeters).

The distance between the tool and the workpiece was monitored by recording the current transient flowing through the cell. At large distances (≥ 20 μm), the current followed the voltage pulse (Fig. 2), indicating no significant charging of the electrodes' DL. Only at distances ≤ 1 μm between the flattened face of the wire and the Cu surface peaking of the current signaled local charging of the DL capacity. Therefore, the height of the current peak directly monitors the tool-workpiece separation, which can be used in a feedback loop for automated adjustment of the gap width between the electrodes. The pause between two pulses was long enough to ensure complete discharge of the DL. Furthermore, adjusting the workpiece potential to the $\text{Cu}|\text{Cu}^{2+}$ equilibrium potential avoids the redeposition of dissolved Cu. During the pulse, the dissolution rate far exceeds the redeposition rate during the pause of the pulse, which

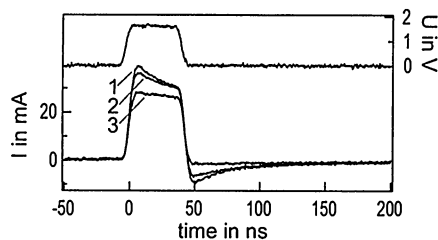


Fig. 2. Single voltage pulse (U) applied to the electrodes and resulting current transients (I) for different electrode separations (1, < 1 μm ; 2, 1 μm ; 3, 20 μm). At small distances below 1 μm , the peaking of the current indicates local charging of the DL in proximity to the face of the tool electrode.

is essentially determined by the exchange current density of the $\text{Cu}|\text{Cu}^{2+}$ redox system (20). This strong asymmetry leads to a net dissolution of Cu.

A scanning electron micrograph of a structure machined into a mechanically polished, electrochemically deposited Cu layer of an electronic circuit board in a solution of 0.01 M HClO_4 and 0.1 M CuSO_4 is shown (Fig. 3A), in which a Pt cylinder (a polished Pt wire 10 μm in diameter) was used as a tool. To obtain the delicate Cu prism in the middle of the hole (cross section, 5 μm by 10 μm ; height, 12 μm), sitting on a pedestal 15 μm by 15 μm by 10 μm , the tool was first etched vertically, 12 μm deep, into the workpiece. This took about 200 s. After "drilling" this ver-

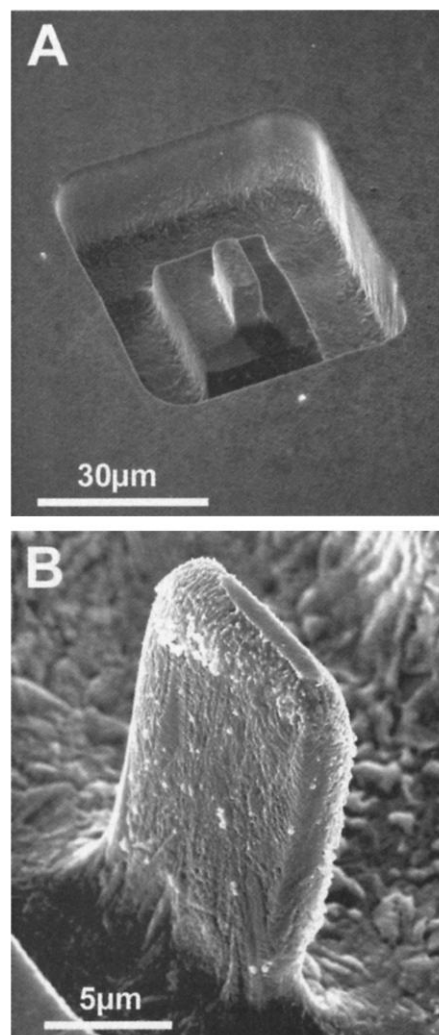


Fig. 3. (A) Cu structure (small prism, 5 μm by 12 μm) machined into the Cu sheet of an electronic circuit board upon application of a 2-MHz sequence of 50-ns, -1.6 -V pulses to the tool electrode (a cylindrical Pt wire 10 μm in diameter) in 0.01 M HClO_4 and 0.1 M CuSO_4 . The tool was first etched vertically into the surface and was then moved along a rectangular path like a miniature milling cutter. (B) Cu tongue with a thickness of 2.5 μm , etched as in (A).

tical hole, the tool was moved laterally along a rectangular path in the Cu sheet like a miniature milling cutter. Then the outer rectangular trough was etched with a total depth of 22 μm . The width of the trough amounted to 14 μm . The complete machining time for the structure was 30 min. While feeding the tool, the minimum distance between tool and workpiece was adjusted to about 0.5 μm by in situ monitoring of the charging peak of the current transient. The well-defined shape of the internal structure and the vertical walls clearly demonstrate the high aspect ratio and precision of the structures achievable with our technique. The radius of curvature at the edges of the hole is less than 0.5 μm . Figure 3B shows a high-magnification image of a very thin Cu tongue (2.5 μm by 10 μm by 15 μm) realized in a similar manner. The parallelism of the side walls is on the submicrometer scale. The fragility of the structure demonstrates the gentle removal of the material without mechanical stress and deformation.

To obtain a more quantitative understanding of the machining performance, the spatial variations of the voltage drop across the workpiece DL were simulated for a cylindrical tool electrode in front of a planar workpiece surface (inset, Fig. 4A). For simplicity, the calculation was performed

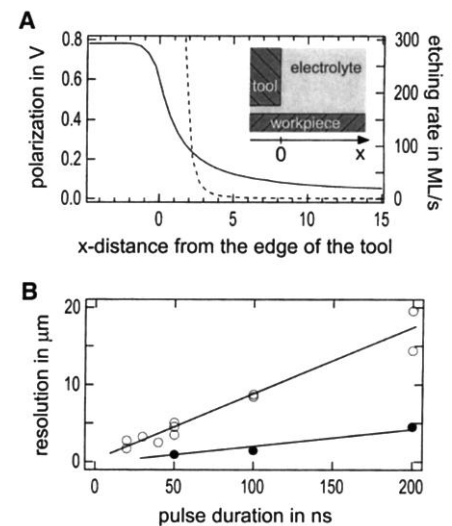


Fig. 4. (A) Solid line: Calculated polarization of the DL on the workpiece at the end of a 50-ns, -1.6 -V pulse applied to a cylindrical tool electrode versus the distance from the edge of the tool. Dashed line: Corresponding Cu dissolution rate. (The zero of the x axis is located at the edge of the tool, as sketched in the inset.) (B) Experimentally determined spatial resolution for various pulse durations and for two different electrolyte concentrations (open circles, 0.09 M HClO_4 and 0.01 M CuSO_4 ; solid circles, 0.01 M HClO_4 and 0.01 M CuSO_4). The resolution is linearly dependent on both the pulse duration and the electrolyte concentration.

for a 2D system, neglecting the curvature of the tool electrode. We calculated the transients of the polarization of the workpiece DL, depending on the distance from the edge of the tool. The resulting polarization of the DL of the workpiece at the end of a 50-ns, -1.6 -V pulse to the tool electrode is displayed in Fig. 4A (DL capacity, $10 \mu\text{F}/\text{cm}^2$; specific electrolyte resistivity, $70 \text{ ohm} \cdot \text{cm}$ (19)). The gap between the face of the tool and the workpiece surface was set to $0.4 \mu\text{m}$. Although the DL directly facing the tool is polarized to almost half of the applied voltage, the polarization steeply drops within the first $2 \mu\text{m}$ outside of the tool edge. As the resting potential of the surface is potentiostatically adjusted to the $\text{Cu}|\text{Cu}^{2+}$ equilibrium potential, the polarization directly corresponds to the overpotential η for Cu dissolution. The corresponding (time- and distance-dependent) etching rate was calculated from the polarization transients, assuming simple Tafel behavior for the dissolution current i_{diss} [$i_{\text{diss}} = i_0 \exp(\alpha\eta/kT)$ with a transfer coefficient of $\alpha = 0.5$ and an exchange current density $i_0 = 1 \text{ mA}/\text{cm}^2$ (20)]. Integration over the pulse length of 50 ns and normalization to the pulse/pause ratio of 1/10 yields the total etching rate (dashed line in Fig. 4A). Because of its exponential dependence on the overpotential, the etching rate exhibits an even steeper decrease than the polarization with increasing distance from

the tool edge. To drill a hole of about $10 \mu\text{m}$ depth within 200 s, the Cu dissolution rate has to be about 200 monolayers (MLs) per second. This corresponds to the experimentally determined rate in the experiment of Fig. 3A, with the experimental parameters comparable to those used in the simulation. The calculated rate in Fig. 4A falls far below that value already at distances beyond $2 \mu\text{m}$ from the tool edge. At $4 \mu\text{m}$ distance, the etching rate dropped to ≈ 2 MLs/s, yielding a dissolution of only 90 nm of Cu within 200 s. Therefore, the surface remains negligibly etched a few micrometers apart from the tool electrode, whereas opposite to its face the surface is strongly etched. This is consistent with the experimentally found width of the trough of $14 \mu\text{m}$ (Fig. 3A), machined with a $10\text{-}\mu\text{m}$ tool, resulting in an effective distance between the tool and the wall of the trough of $2 \mu\text{m}$. The achievable machining precision is much better than the width of that gap and is mainly determined by the steep decrease of the etching rate (Fig. 4A). In the above calculation, diffusion-limited mass transport of Cu ions was neglected. Outside of the small gap between tool and workpiece, this assumption is certainly valid because of the overall low Cu dissolution rate and the unrestricted access to the bulk of the electrolyte. However, in the small gap in front of the tool face, limited diffusion lowers the effective etching rate to a value significantly lower than that expected from the high local overpotential with simple Tafel behavior.

The resolution found in both simulation and experiment fits well with the rough approximation employing the time constant τ of the DL charging. (With the experimental parameters employed, the resolution d approximates to $d \approx \tau/c_{\text{DL}}\rho \approx 1.4 \mu\text{m}$.) From the linear correlation between time constant τ , specific electrolyte resistance ρ , and spatial resolution d , it can be conjectured that lowering the electrolyte concentration or shortening the pulse duration should linearly increase the machining precision. To quantitatively check the dependence of the spatial resolution on the experimental parameters, we performed etching experiments on a Cu film $0.5 \mu\text{m}$ thick. The film was deposited onto a Au substrate in the electrochemical cell before the machining by short voltage pulses. For this experiment, a cylindrical, flattened, Pt wire $50 \mu\text{m}$ in diameter was used as a tool. It was held at submicrometer distance in front of the Cu film. It took about 10 s to etch through the Cu film. Afterward, the hole diameter continuously increased, until after about 100 s the lateral etching effectively ceased. This is due to the steeply decreasing etching rate with increasing distance

from the edge of the tool, as pointed out in Fig. 4A. This experiment was repeated with varying pulse durations and electrolyte concentrations. In Fig. 4B, the experimental spatial resolution [(final hole diameter – tool diameter)/2], resulting after an etching time of 10 min, is plotted for different pulse durations and two different electrolyte concentrations with specific electrolyte resistances of $30 \text{ ohm} \cdot \text{cm}$ (0.09 M HClO_4 and 0.01 M CuSO_4) and $150 \text{ ohm} \cdot \text{cm}$ (0.01 M HClO_4 and 0.01 M CuSO_4) (19). In agreement with the prediction, for both concentrations the spatial resolution scales linearly with the pulse duration, as indicated by the guides to the eye. The slopes of the lines differ by a factor of ≈ 5 , which corresponds to the ratio of the conductivities of the two electrolytes. Thus, the machining precision can be significantly enhanced over that demonstrated in Fig. 3 simply by reducing the pulse duration or the electrolyte concentration. The only constraint is the presence of a sufficient amount of electrolyte ions in the small gap between the electrodes in order to enable the buildup of the polarization of the DL. Upon polarization of the DL of a typical metal surface (DL capacity $\approx 10 \mu\text{F}/\text{cm}^2$) by 1 V, about 0.1 MLs of ions are consumed. According to the above approximation, application of 100-ps pulses in a 0.3 M electrolyte should theoretically lead to a spatial resolution in the 10-nm range.

Electrochemical machining with ultrashort voltage pulses can in principle be applied to all electrochemically active materials, including semiconductors. This is demonstrated with *p*-Si in 1% hydrofluoric acid (HF) (Fig. 5A). A flattened $50\text{-}\mu\text{m}$ Pt wire was vertically etched into the surface upon application of 200-ns, -0.5 -V pulses. However, because of the complexity of the possible electrochemical reactions, appropriate parameters of pulse height and electrochemical potential of the surface had to be selected. Pulses that are too high may lead to passivation of the surface by the formation of Si oxides. Additionally, both type and concentration of the dopant are of crucial influence on electrochemistry, conductivity of the Si, and capacity of the DL (21). For proper machining, all of these parameters have to be taken into account.

The reversal of electrochemical reactions offers additional possibilities for microstructuring. Not only local dissolution but also local deposition of material can be achieved (Fig. 5B). A series of Cu dots was locally deposited from a 0.01 M HClO_4 and 0.1 M CuSO_4 electrolyte onto a Au film by the application of positive pulses (400 ns, 2 V) to the tool. The overall potential of the Au surface was kept at the equilibrium

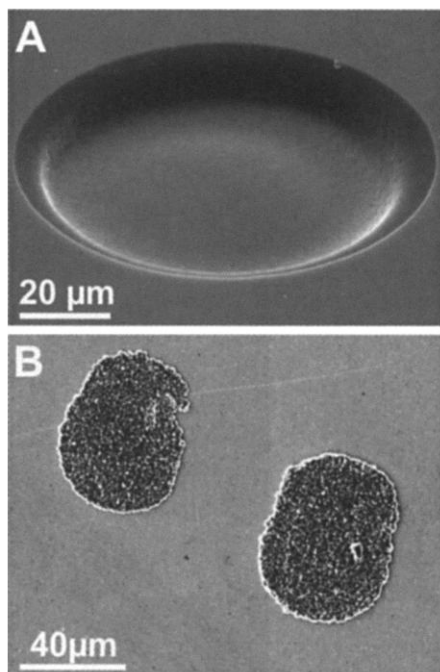


Fig. 5. (A) Hole etched into *p*-Si with a cylindrical $50\text{-}\mu\text{m}$ Pt tool in 1% HF (with 200-ns, -0.5 -V pulses to the tool). (B) Cu dots deposited on a Au substrate with an elliptical Pt tool $50 \mu\text{m}$ in diameter in 0.01 M HClO_4 and 0.1 M CuSO_4 (with 400-ns, 2-V pulses).

potential of the Cu|Cu²⁺ redox system, thus preventing the large-scale deposition of Cu as well as the dissolution of the deposited Cu dots. An elliptical Pt wire about 50 μm in diameter was used as a tool, which is reflected in the elliptical shape of the dots. For the formation of Cu crystallites on the Au surface, a nucleation barrier has to be surmounted (22), requiring a critical Cu adatom concentration on the Au surface during the pulse. This kinetic constraint assists the strongly localized Cu deposition.

The versatility of electrochemical reactions, combined with spatial resolution down to the nanometer range, may provide new abilities for modern micromachining technologies. Electrochemical microstructuring is not restricted to sequential fabrication. Complicated structures could be molded directly onto a surface using an

appropriately shaped tool. The theoretically achievable spatial resolution compares favorably with that of state-of-the-art lithographical techniques, with the additional advantage of fully 3D capabilities.

References and Notes

1. P. Rai-Coudhury, Ed., *Handbook of Microlithography, Micromachining, & Microfabrication* (SPIE Optical Engineering Press, Bellingham, WA, 1997).
2. I. Amato, *Science* **282**, 402 (1998).
3. M. A. Burns et al., *Science* **282**, 484 (1998).
4. J. T. Santini, M. J. Cirna, R. Langer, *Nature* **397**, 335 (1999).
5. H. Jerman and S. Terry, in (1), vol. 2, pp. 379–434.
6. M. U. Kopp, A. J. d. Mello, A. Manz, *Science* **280**, 1046 (1998).
7. K. Jensen, *Nature* **393**, 735 (1998).
8. C. R. Friedrich et al., in (1), vol. 2, pp. 299–378.
9. R. M. Nyffenegger and R. M. Penner, *Chem. Rev.* **97**, 1195 (1997).
10. A. J. Bard, G. Denuault, C. Lee, D. Mandler, D. O. Wipf, *Acc. Chem. Res.* **23**, 357 (1990).
11. W. Li, J. A. Virtanen, R. M. Penner, *Appl. Phys. Lett.* **60**, 1181 (1992).

12. W. Li et al., *J. Phys. Chem.* **100**, 20103 (1996).
13. R. T. Pötzschke, C. A. Gervasi, S. Vinzelberg, G. Staikov, W. J. Lorenz, *Electrochim. Acta* **40**, 1469 (1995).
14. R. Schuster, V. Kirchner, X. H. Xia, A. M. Bittner, G. Ertl, *Phys. Rev. Lett.* **80**, 5599 (1998).
15. D. Hoffmann, W. Schindler, J. Kirschner, *Phys. Rev. Lett.* **73**, 3279 (1998).
16. D. M. Kolb, R. Ullmann, T. Will, *Science* **275**, 1097 (1997).
17. C. Lebreton and Z. Z. Wang, *J. Vac. Sci. Technol. B* **14**, 1356 (1996).
18. P. Avouris, T. Hertel, R. Martel, *Appl. Phys. Lett.* **71**, 285 (1997).
19. G. Milazzo, *Electrochemistry* (Elsevier, Amsterdam, 1963).
20. J. O. M. Bockris and A. K. N. Reddy, *Modern Electrochemistry* (Plenum, New York, 1970), vol. II.
21. H. Gerischer, *Electrochim. Acta* **35**, 1677 (1990).
22. M. A. Schneeweiss and D. M. Kolb, *Phys. Stat. Sol. (a)* **153**, 51 (1999).
23. We thank K. Grabitz, G. Heyne, J. Lehnert, and V. Platschkowski for technical support and D. Kolb for discussions.

5 April 2000; accepted 19 May 2000

Taming Superacids: Stabilization of the Fullerene Cations HC₆₀⁺ and C₆₀^{·+}

Christopher A. Reed,* Kee-Chan Kim, Robert D. Bolskar, Leonard J. Mueller

A new superacid, H(CB₁₁H₆X₆) (where X = chlorine or bromine), whose conjugate base is the exceptionally inert CB₁₁H₆X₆⁻ carborane anion, separates Brønsted acidity from oxidizing capacity and anion nucleophilicity in a manner not previously achieved. Reaction of this superacid with C₆₀ gives HC₆₀⁺ as a stable ion in solution and in the solid state. In a separate experiment, an oxidant was developed such that the long-sought C₆₀^{·+} ion can be synthesized in solution. The preparation of these two fullerene carbocations is a notable departure from the prevalent chemistry of C₆₀, which is dominated by the formation of anions or the addition of nucleophiles. The H(CB₁₁H₆X₆) superacid overcomes the major limitations of presently known superacids and has potentially wide application.

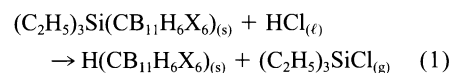
Superacids (those stronger than 100% sulfuric acid) have been of great value to chemistry. In organic chemistry, superacidity has been used to stabilize carbocations such as R₃C⁺ and HCO⁺ and to study acid-catalyzed processes (1, 2). In inorganic chemistry, the oxidizing capacity of superacids has been widely exploited to stabilize unusual reactive cations such as S₈²⁺, Ir(CO)₆³⁺, and Xe₂⁺ (3–6). Nevertheless, currently known superacids have limitations. For example, the anions of superacids (SbF₆⁻, HSO₄⁻, CF₃SO₃⁻, and so forth) are too nucleophilic to allow the free silylium ion (R₃Si⁺) to exist (7), and attempts to protonate and/or oxidize C₆₀ with

superacids have led to its decomposition (8). Indeed, it is the combination of anion nucleophilicity and oxidizing capacity together with acidity that makes superacids corrosive and destructive, and limits many academic and industrial applications. Even the ostensibly nonoxidizing superacid triflic acid (CF₃SO₃H) decomposes C₆₀ (9).

If a superacid could be developed which was oxidant-free and whose conjugate base was significantly less nucleophilic than presently available anions, many desirable protonation reactions might be carried out without decomposition. Here, we report the preparation of a superacid, H(CB₁₁H₆X₆) (X = Cl, Br), that meets these requirements and illustrate its use in stabilizing the previously unobserved HC₆₀⁺ ion. We also show that the oxidizing capacity of superacids can be separately harnessed to the conjugate base

(CB₁₁H₆X₆⁻) to prepare an oxidant capable of producing the C₆₀^{·+} cation. C₆₀ has been referred to as the “electrophile par excellence” (10) because its dominant chemistry is the addition of nucleophiles or electrons (for example, C₆₀ⁿ⁻ for n = 1 to 6). Thus, the addition of an electrophile or the removal of an electron to form HC₆₀⁺ and C₆₀^{·+}, respectively, presents a particular challenge for synthetic chemistry and an excellent test for the concept of strict separation of oxidation from acidity and nucleophilicity.

Superacidity can be generated from a non-superacidic Brønsted acid by addition of a strong Lewis acid. A typical example is the addition of SbF₅ to HF to generate the common superacid HSbF₆, properly formulated as [H(HF)_x]⁺[nSbF₅·SbF₆]⁻ (4). Here, we exploit the potent Lewis acidity of the silylium ion (R₃Si⁺) to generate superacidity from HCl. Latent silylium ions are found in the silylium ion–like species R₃Si(CB₁₁H₆X₆) (7) where CB₁₁H₆X₆⁻ is the exceptionally inert and weakly nucleophilic anion shown in Fig. 1 (11). Condensing liquid HCl onto solid (C₂H₅)₃Si(CB₁₁H₆X₆) at low temperature followed by removal of the volatiles under vacuum at room temperature yields the desired acid H(CB₁₁H₆X₆) in essentially quantitative yield (Eq. 1).



The absence of a AgCl precipitate when the product is dissolved in aqueous AgNO₃ shows that the possible alternative formulation of a HCl-solvated proton in [H(HCl)_x]⁺[CB₁₁H₆X₆]⁻ can be discounted. For X = Br, the acid can be successfully sublimed under vacuum (10⁻⁷ kPa) at 185°C to give a reasonable yield (45%) of white crystalline solid

Department of Chemistry, University of California, Riverside, CA 92521–0403, USA.

*To whom correspondence should be addressed. E-mail: chris.reed@ucr.edu